Source-explicit estimation of brown carbon in the polluted atmosphere over North China Plain: implications for distribution, absorption and direct radiative effect

Jiamao Zhou[1,2], Jiarui Wu[1], Xiaoli Su[1], Ruonan Wang[1], Imad EI Haddad[4], Xia Li[1], Qian Jiang[1], Ting Zhang[1], Wenting Dai[1], Junji Cao[3], Andre S.H. Prevot[4], Xuexi Tie[1], Guohui Li[1]

[1]Key Laboratory of Aerosol Chemistry and Physics, State Key Laboratory of Loess and Quaternary Geology, Institute of Earth Environment, Chinese Academy of Sciences, Xi'an 710061, China

[2]Guanzhong Plain Ecological Environment Change and Comprehensive Treatment National Observation and Research Station, Xi'an 710061, China

[3]Institute of Atmospheric Physics, Chinese Academy of Sciences, Beijing 100029, China

[4]PSI Center for Energy and Environmental Sciences, Paul Scherrer Institute, 5232 Villigen, Switzerland

Correspondence to: Guohui Li (ligh@ieecas.cn)

Abstract. Brown carbon (BrC) plays a significant role in altering atmospheric radiation. Beyond biomass and biofuel combustion, recent studies identify fossil fuel sources—especially residential coal burning and vehicle exhaust—as major contributors to BrC. This underscores a gap in climate models, which often assume fossil fuel organic aerosols (OA) are non-absorbing or treat all OA as light-scattering. In this study, we simulate BrC over the North China Plain (NCP) during a winter pollution event using the WRF-Chem model, incorporating explicit BrC absorption properties. The model aligns well with observed pollutant and aerosol levels, revealing an average near-surface BrC concentration of 5.2 μg m^{-3}, contributing 16.4% to aerosol absorption at 365 nm. Using a diagnostic adjoint approach, we estimate that BrC exerts a direct radiative effect (DRE) averaging -0.09 W m^{-2} at the top of the atmosphere, reducing the cooling effect of organic carbon by 28.0% and producing a local warming effect of up to +0.40W m^{-2}. Coal combustion is the largest BrC source in the NCP in 2014, though secondary BrC also significantly impacts the regional radiation balance.

Key words: Brown Carbon, emission sources, absorption, direct radiative effect

1 Introduction

Brown Carbon (BrC) is a collective component for those colored organic compounds with wavelength dependent light-absorption properties (Mukai and Ambe, 1986; Kirchstetter et al., 2004; Andreae and Gelencsér, 2006). BrC has been recognized as an important short-lived climate forcer contributing considerably to climate change by warming of the atmosphere (IPCC, 2013; Feng et al., 2013; Jacobson, 2014; Jo et al., 2016; Brown et al., 2018). A study suggested that the light absorption induced by BrC can be equal to or even higher than that of black carbon (Pokhrel et al., 2017), and substantially influences atmospheric radiative forcing. Recent studies have shown that BrC accounts for 30%~50% of the total absorption of aerosols in Atlanta USA, Brazil and Hebei China (Hoffer et al., 2006; Yang et al., 2009; Liu et al., 2013). The direct radiation effect (DRE) caused by BrC is greater than +1 W m^{-2} in some regions, such as South Asia, Africa and Southeast Asia, much higher than the global average (Park et al., 2010; Feng et al., 2013; Lin et al., 2014; Saleh et al., 2014; Jo et al., 2016; Wang et al., 2018; Yan et al., 2018). However, the modelled DRE associated with BrC remains highly uncertain, with variations spanning an order of magnitude difference. In particular, the estimated global DRE of BrC is in the range between +0.03 W/m^2 to +0.57 W/m^2 (Hammer et al., 2016), which is caused by the limited observations of BrC mass and absorption properties (Tuccella et al., 2020; Saleh, 2020).

It has been well established that BrC is not a single substance, but a general term for light-absorbing organic aerosols. A series of laboratory measurements and observations in the earlier years demonstrate that BrC is mainly associated with smoldering biomass burning (BB) or biofuel (BFs) combustion (Chakrabarty et al., 2010; Chen and Bond, 2010; Lack et al., 2012; Washenfelder et al., 2015; Kumar et al., 2018). On the other hand, OA from fossil-fuel combustion are generally assumed to be non-absorbing as the combustion conditions for fossil fuels (FFs) are typically not conducive for BrC formation (Hecobian et al., 2010; Shapiro et al., 2009; Bond et al., 2013). Therefore, earlier climate model studies have assumed that primary OA from BB and BFs combustion is the main or sole BrC source (Feng et al., 2013; Jacobson, 2014; Saleh et al., 2014; Hammer et al., 2016; Brown et al., 2018). Recent studies have also incorporated the ageing of secondary organic aerosol (SOA) (Jo et al., 2016; Wang et al., 2018; Zhang et al., 2020). However, more recent exceptions are being found in low-efficiency residential-coal combustion (RCC) (Bond, 2001; Yan et al., 2017; Xie et al., 2019; Tian et al., 2019; Zhang et al., 2022a) and fuel-oil combustion in vehicle and ship engines (Xie et al., 2017; Corbin et al., 2019; Tang et al., 2020; Huang et al., 2022). It is now generally accepted that the formation of BrC is not exclusively linked to the chemical make-up of biomass fuels but is most critically determined by the combustion conditions (Saleh et al., 2018; Cheng et al.,

2020; Saleh, 2020; Wang et al., 2022a). The key factor contributing to the high levels of BrC observed from biomass fuels is their combustion under relatively low-temperature and fuel-rich conditions, which are highly favorable for BrC formation. In contrast, fossil fuels, such as those burned in internal combustion engines, typically undergo combustion at higher temperatures and under more fuel-lean conditions, which are less conducive to BrC production (Saleh, 2020). China, as a developing country, coal is commonly used for residential heating in cold season, causing massive emissions of organic particles (Yan et al., 2017; Li et al., 2018). According to the National Bureau of Statistics of China (https://data.stats.gov.cn), the coal consumption in 2014 was about 4000 Tg, accounting for 65.8% of the total primary energy use of China. Of this, around 93 Tg is used as household fuel. The poor burning conditions and limited emission control facilities in this region could lead to substantial emissions of BrC. This could explain why, to date, all reported instances of coal-derived BrC have originated from China. Both Yan et a., (2017) and Mo et al., (2021) have used dual carbon isotope-based source apportionment method reported that fossil fuel, especially coal combustion from the residential sector is important source in northern China, even the largest contributor in some regions.

These recent findings indicate a critical gap on the treatment of BrC in chemical transport models, atmospheric chemistry models and climate models as well, which present an even greater concern, as they typically do not consider BrC at all (Ma et al., 2021; Jo et al., 2023; Gao et al., 2025; Ge et al., 2025). Addressing this gap requires expanding the scope of BrC sources, assigning distinct optical properties for each source and incorporating those that have been underrepresented or overlooked in past assessments into numerical models. In this study, we include the main primary emission sources (RCC, BB, BFs, FFs-TRA) of BrC and secondary derived BrC in a regional model, the Weather Research and Forecasting model coupled with Chemistry (WRF-Chem). A representative region, North China Plain (NCP), is chosen as the study domain with high anthropogenic carbonaceous aerosols due to the widespread use of coal and biomass burning for heating during winter and the increasing number of motor vehicles. We performed a month simulation to evaluate the surface distribution, absorption and the DRE of BrC in the NCP, by updating BrC optical properties of different sources. Sensitivity experiments have also been devised to assess the contribution of BrC from major sources.

2 Model and Method

2.1 WRF-Chem Model and configurations

The WRF-Chem model (Grell et al., 2005; Fast et al., 2006) modified by Li et al., (2010; 2011a; 2011b; 2012) is used to quantitatively estimate the BrC in the NCP. A heavily polluted month from January 1 to 30, 2014 is

87 selected for the simulation period. The anthropogenic emissions are developed by Zhang et al. (2009) and Li et al.

88 (2017), including five sources, namely agriculture, industry, power generation, residential, and transportation. The

89 biogenic emissions are calculated online using the MEGAN (Model of Emissions of Gases and Aerosol from

90 Nature) model developed by Guenther et al. (2006). Additionally, the grid-based RCC, BB and BFs combustion

91 emissions are used to update the BrC sources in this study, described later. The model simulation domain is shown

92 in Fig. 1. The detailed model description and configurations can be found in supplementary text S1 and Table S1,

93 respectively.

94
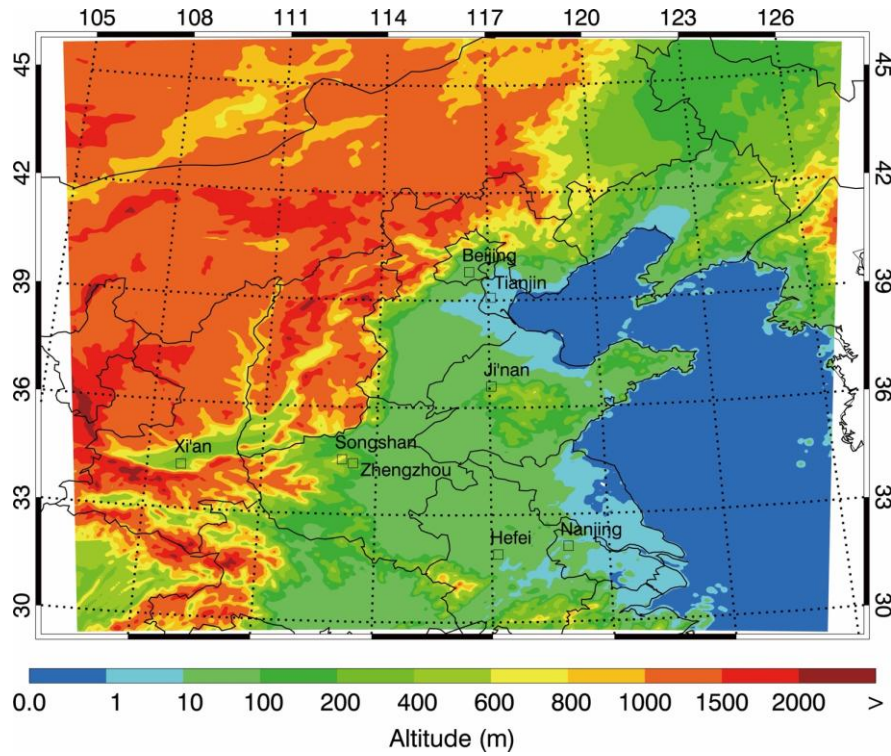
95 **Figure 1. WRF-Chem simulation domain with topography. The square denotes the field sites for simulation and**
96 **observation comparison**

97 **2.2 Aerosol radiative module**

98 The aerosol radiative module developed by Li et al., (2011a) has been incorporated into the WRF-Chem

99 model to calculate the aerosol optical depth (AOD or τ_a), single scattering albedo (SSA or ω_a), and the

100 asymmetry factor (g_a). In the aerosol module, aerosols are represented by a three-moment approach with a

101 lognormal size distribution:

102 $n(lnD) = \frac{N}{\sqrt{2\pi}ln\sigma_g} exp[-\frac{1}{2}(\frac{lnD-lnD_g}{ln\sigma_g})^2]$ (1)

103 Where D is the particle diameter, N is the number distribution of all particles in the distribution, D_g is the

104 geometric mean diameter, and σ_g is the geometric standard deviation. To calculate the aerosol optical properties,

105   the aerosol spectrum is divided into 48 bins from 0.002 to 20.0 μm, with radius r_i. The aerosols are classified

106   into four types: (1) internally mixed sulfate, nitrate, ammonium, hydrophilic organics and black carbon (BC), and

107   water; (2) hydrophobic organics; (3) hydrophobic BC; and (4) other unidentified aerosols (generally dust-like

108   aerosols). These four kinds of aerosols are assumed to be mixed externally. For the internally mixed aerosols, the

109   complex refractive index at a specific wavelength (λ) is calculated based on the volume-weighted average of the

110   individual refractive index. Given the particle size and complex refractive index, the extinction efficiency (Q_e),

111   ω_a and g_a are calculated using the Mie theory at a certain wavelength (λ). The look-up tables of Q_e, ω_a and

112   g_a are established according to particle sizes and refractive indices to avoid multiple Mie scattering calculation.

113   The aerosol optical parameters are interpolated linearly from the look-up tables with the calculated refractive

114   index and particle size in the module. The τ_a at a certain λ in a given atmospheric layer k is determined by

115   the summation over all types of aerosols and all bins:

116     $$\tau_a(\lambda, k) = \sum_{i=1}^{48}\sum_j^4 Q_e(\lambda, r_i, j, k)\pi r_i^2 n(r_i, j, k)\Delta Z_k \qquad (2)$$

117   where $n(r_i, j, k)$ is the number concentration of j-th kind of aerosols in the i-th bin. ΔZ_k is the depth of an

118   atmospheric layer. The weighted-mean values of ω_a and g_a are then calculated by using D'Almeida et al.,

119   (1991):

120     $$\omega_a(\lambda, k) = \frac{\sum_{i=1}^{48}\sum_j^4 Q_e(\lambda, r_i, j, k)\pi r_i^2 n(r_i, j, k)\omega_a(\lambda, r_i, j, k)\Delta Z_k}{\sum_{i=1}^{48}\sum_j^4 Q_e(\lambda, r_i, j, k)\pi r_i^2 n(r_i, j, k)\Delta Z_k} \qquad (3)$$

121     $$g_a(\lambda, k) = \frac{\sum_{i=1}^{48}\sum_j^4 Q_e(\lambda, r_i, j, k)\pi r_i^2 n(r_i, j, k)\omega_a(\lambda, r_i, j, k)g_a(\lambda, r_i, j, k)\Delta Z_k}{\sum_{i=1}^{48}\sum_j^4 Q_e(\lambda, r_i, j, k)\pi r_i^2 n(r_i, j, k)\omega_a(r_i, j, k)\Delta Z_k} \qquad (4)$$

122   When the wavelength-dependent τ_a, ω_a, and g_a are calculated, they can be used in the Goddard shortwave

123   module.

124   It is worth noting that the aerosol liquid water content in the study is predicted with the inorganic

125   aerosols using a computationally efficient thermodynamic equilibrium model, ISORROPIA (version 1.7,

126   (Nenes et al., 1998; Fountoukis and Nenes, 2007). In this study, ISORROPIA is mainly used to predict the

127   thermodynamic equilibrium between the ammonium-sulfate-nitrate-chloride-water aerosols and their gas-phase

128   precursors H_2SO_4-HNO_3-NH_3-HCL-water vapor, and water uptake of aerosols is calculated using the Zdanovskii-

129   Stokes-Robinson (ZSR) correlation (Stokes and Robinson, 1966):

130     $$W = \sum_i \frac{M_i}{m_{oi}(a_w)} \qquad (5)$$

131   Where W is the mass concentration of aerosol liquid water (kg m^{-3} air), M_i is the molar concentration of

132   species i (mol m^{-3} air), and $m_{oi}(a_w)$ is the molality of an aqueous binary solution of the i-th electrolyte

133   with the same a_w (i.e. relative humidity) as in the multicomponent solution.

134   The BrC in the model has an effective density of 1.2 g cm^{-3} for primary BrC (Turpin and Lim, 2001) and of

135   1.0 g cm^{-3} for secondary BrC (Hurley et al., 2001). The imaginary refractive index of BrC used in this study is

136   discussed in 2.3.2.

2.3 Model modifications

2.3.1 Source separation of BrC

139   The definition of BrC in the model is dependent on its sources. Due to the lack of BrC emission inventories,

140   According to the characteristics of energy structure in China, assumptions and code modifications of the WRF-

141   Chem model have been made to consider the BrC from different sources. These involve three separated primary

142   BrC sources, including BB emissions, FFs emissions from RCC and on-road vehicles (FFs-TRA), and a part of

143   SOA which has light absorption property whereas other types of primary OA (POA) and SOA are assumed to be

144   purely scattering. In this study, BB source corresponds to open fire, household biomass burning and biofuel

145   consumption emissions.

146   For the primary emissions, previous BrC simulations have substituted it with a proportion of POA directly

147   (Feng et al., 2013; Lin et al., 2014; Wang et al., 2014; Tuccella et al., 2020; Xu et al., 2024) , derived it from the

148   relationship between the burning efficiency and the observed aerosol light absorption (Jo et al., 2016; Zhu et al.,

149   2021), or determined it through parameterization where BrC absorption is a function of the BC-to-OA emission

150   ratio (Zhang et al., 2020). In the present work, we calculated the primary BrC emissions based on the bottom-up

151   OA emission inventory combined with reported annual BrC emissions from various primary sources, as shown in

152   Table 1. Firstly, we collected the reported annual emissions of BrC from RCC, BB and FFs-TRA by using bottom-

153   up inventory method. It should be noted that given the proximity of the study period (January 2014) to 2013, we

154   use the emissions of BrC from RCC and BB in 2013 provided by Sun et al., (2017; 2021), which is 592Gg and

155   712Gg, respectively. The emissions of FFs-TRA derived BrC is 76Gg, which is calculated based on the value of

156   2017 (Wang et al., 2022a)and scaled by a factor of 0.70 to reflect the change of annual civilian-owned motor

157   vehicles. We assume that the spatial and seasonal variation of BrC is similar to OA. Then bottom-up emissions

158   inventory induced monthly BrC emissions in the NCP in January 2014 is the annual BrC emissions multiplied by

159   the ratio of OA emissions in NCP *vs* China, and the ratio of OA emissions in January 2014 *vs* the whole year,

160   resulting in a value of 65.5 Gg, 56.8 Gg and 4.4 Gg for RCC, BB and FFs-TRA, respectively. Finally, the

161   proportion of the three primary emissions of BrC used in the model is 36.3%, 100.8% and 15.8%, respectively.

162   Figure 2 shows the contributing regions and burdens of the three separated primary sources of BrC.

163 **Table 1 The data for primary BrC emissions calculation**

Primary sources of BrC	RCC	BB	FFs-TRA
Annual BrC emissions (Gg) in China	592.0[a]	712.0[b]	76.0[c]
Ratio of OA emissions in the NCP vs China[e]	57.7%	51.0%	69.4%
Ratio of OA emissions in January 2014 vs the whole year[e]	19.2%	14.0%	8.3%
Bottom-up emissions inventory induced monthly BrC emissions in the NCP in January	65.5	56.8[d]	4.4
Emissions in the NCP in January 2014[e]	180.2	56.4	27.9
BrC emissions ratio for primary sources used in the model	36.3%	100.8%	15.8%

164 [a] The BrC emissions from China's RCC in 2013 was reported by Sun et al., (2017) based on experiments involving seven coals

165 were burned in four typical stoves as both chunk and briquette styles.

166 [b] The calculated BrC emissions from China's household biomass burning in 2013 reported by Sun et al., (2021) using 11 widely

167 used biomass types in China burned in a typical stove.

168 [c] The estimated BrC emissions from vehicle exhaust in 2017 was 109 Gg reported by Wang et al., (2022a). In this study, the

169 emissions of FFs-TRA derived BrC is 76.0 Gg with a yearly scale factor 0.70 which derived by the annual civilian-owned

170 motor vehicles between 2014 and 2017.

171 [d] The value of BrC emissions in NCP in January 2014 is additionally added with OA emitted from the open-biomass burning

172 (6 Gg) which is assumed to be entirely light-absorbing.

173 [e] These values were derived from the OA emission inventory described in Sec. 2.1

174
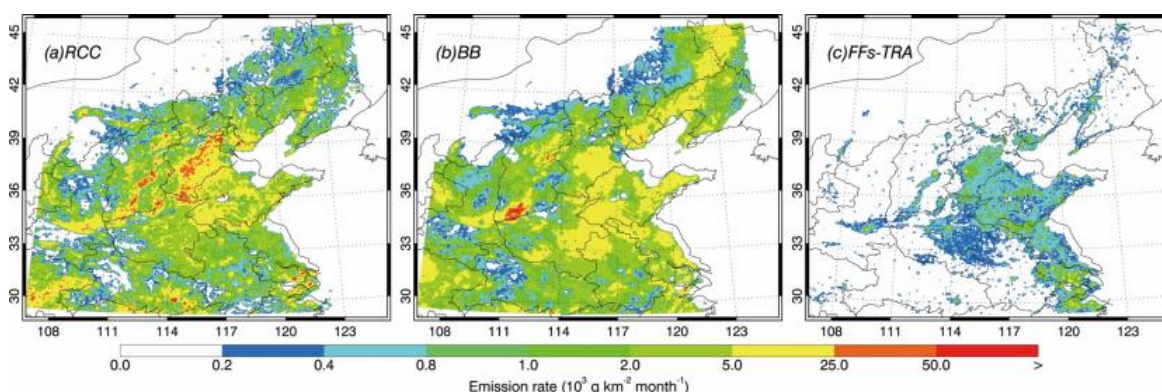
175 **Figure 2 Monthly BrC emissions burdens in January 2014 in NCP from RCC, BB and FFs-TRA.**

176   SOA has also shown light absorption in the atmosphere (Lin et al., 2014). Laboratory experiments have

177 revealed that most of the light-absorbing SOA is associated with aromatic SOA (Jacobson, 1999; Laskin et al.,

178 2015; Li et al., 2020) and the absorption from biogenic SOA in the field has been found to be negligible

179 (Washenfelder et al., 2015) . Therefore, here we assume aromatic derived SOA as secondary BrC in the model

180 following previous studies (Jo et al., 2016; Wang et al., 2018).

181   Moreover, it is worth noting that both primary and SOA light absorption were shown to be dynamic, where

182 BrC can be bleached when they undergo photodissociation (Forrister et al., 2015; Wong et al., 2019), or be darken

183 by cloud and fog processing of aerosols (Moise et al., 2015; Lin et al., 2017; Cheng et al., 2020). These processes

184 are not considered in this study yet. More detailed parameterization of the chemical aging of BrC are needed in

185 future BrC models.

186 **2.3.2 BrC optical properties**

187 The refractive indices of BrC as a function of wavelength are used for radiative transfer calculations. The

188 complex refractive index ($m = n + ik$) of aerosol components enables practical implementation in the model,

189 where n is the real part primarily associated with the scattering efficiency, and k is the imaginary part primarily

190 associated with the absorption efficiency (Bohren and Huffman, 1998). The real part of BrC refractive index is

191 the same of non-absorbing OA which is fairly constrained with reported values typically ranging from 1.5 to 1.7

192 (Saleh et al., 2014; Browne et al., 2019; Li et al., 2020). In this study, it follow the study by Li et al. (2011a) and

193 Wu et al. (2020). The imaginary part (k) of BrC refractive index exhibit strong wavelength dependence and the

194 values range over several orders of magnitude (Saleh et al., 2018; Sengupta et al., 2018). Limited studies on the

195 optical properties of BrC from fossil fuel combustions are reported at present. The average mass absorption

196 efficiency (MAE) of RCC at 365nm is ranging from 0.80 m^2 g^{-1} to 2.47 m^2 g^{-1} (Yan et al., 2017; Li et al., 2019;

197 Tang et al., 2020; Wang et al., 2020; Ni et al., 2021; Song et al., 2021; Wang et al., 2021). In this study, as shown

198 in Table 2, two sets of MAE are used for the sensitivity experiments of BrC. We choose a field optical

199 measurement of BrC from all sources made by Zhang et al., (2022b) as the high absorption case (HI-BRC-

200 ABS) .The optical properties of BB and FFs-TRA obtained in laboratory by Xie et al., (2017), as well as MAE of

201 RCC and secondary BrC obtained in laboratory by Ni et al, (2021) are adopted as the low absorption case (LOW-

202 BRC-ABS) in the study. The imaginary part of the two cases have shown wavelength dependent light-absorption

203 properties and the changes in anthropogenic emissions affect the optical properties of BrC. The imaginary part of

204 both two cases are interpolated to 11 wavelengths to match the aerosol radiation calculation of Goddard module

205 in WRF-Chem. The value of k in this work is derived from the measured MAE using the following Eq.(6) (Liu

206 et al., 2013; Lu et al., 2015) as shown in Table2:

207 $$k_{BrC,\lambda} = \frac{\rho \times \lambda \times MAE_\lambda}{4\pi}$$ (6)

208 Where MAE_λ (m^2 g^{-1}) is the bulk mass absorption efficiency of BrC at the corresponding wavelength λ. ρ (g

209 cm^{-3}) is the density of organic aerosols, which is assigned as 1.2 g cm^{-3} (Turpin and Lim, 2001) in this study.

210

Table 2 The refractive index of BrC used in the model

Aerosols	Wavelength (nm)	k values for HI-BRC-ABS	k values for LOW-BRC-ABS
BrC-RCC	365	-	0.0320
	370	0.1890	-
	470	0.0608	-
	500	-	0.0020
	520	0.0272	-
	590	0.0173	-
	660	0.0081	-
BrC-BB	365	-	0.0300
	370	0.0587	-
	405	-	0.0016
	470	0.0219	-
	520	0.0120	-
	550	-	0.0026
	590	0.0092	-
	660	0.0046	-
BrC-FFs-Tra	365	-	0.0180
	370	0.0509	-
	405	-	0.0130
	470	0.0194	-
	520	0.0085	-
	550	-	0.0045
	590	0.0046	-
	660	0.0018	-
BrC-SOA	365	-	0.0049
	370	0.0251	-
	470	0.0166	-
	500	-	0.0007
	520	0.0114	-
	590	0.0107	-
	660	0.0063	-

'-' means not available

2.3.3 Shortwave direct radiative effect calculation and experimental design

The shortwave DRE calculations of BrC follow the method reported by Chen et al (2021) as shown in Eq. (7). The DRE of BrC is calculated by the difference between the net radiant flux with and without BrC, where the net radiant flux is the difference between the downward $(F_\downarrow)$ and upward radiant flux $(F_\uparrow)$.

$$DRE_{TOA} = \left(F^a_{\downarrow TOA} - F^a_{\uparrow TOA}\right) - \left(F^0_{\downarrow TOA} - F^0_{\uparrow TOA}\right) \tag{7}$$

Where DRE_{TOA} represent the shortwave DRE at the top of the atmosphere (TOA). F^a and F^0 are the radiant flux with and without BrC aerosols, respectively.

An adjoint methodology proposed by Zhao et al (2013) and Huang et al. (2015) has been used to diagnose the optical depth and DRE of BrC aerosols. Optical properties and radiative transfer of different sources BrC are calculated multiple times with one or a group of aerosol mass removed or without BrC absorption from each calculation following Eq. (8) and Eq. (9). In addition, the model also takes into account the reduced aerosol masses

225   along with the change in aerosol number concentration and size distribution.

226     $AOD_{[species\ i]} = AOD_{[all\ species]} - AOD_{[without\ species\ i/without\ species\ i\ absorption]}$ (8)

227     $DRE\ Forcing_{[species\ i]} = DRE\ Forcing_{[all\ species]} - DRE\ Forcing_{[without\ species\ i/without\ speices\ i\ absorption]}$ (9)

228   This method is more efficient than the traditional approach of running the model multiple times with the

229   exclusion of a specific aerosol component. It not only saves computational time but also provides a more accurate

230   estimation focused solely on the direct radiative effect of aerosols.

231   **3 Results and Discussions**

232   **3.1 Model performance**

233   Before evaluating the DRE of BrC, results from the standard simulation are used to validate the model

234   performance. Using available measurements, we first validate the spatial distribution and temporal variation of

235   air pollutants ($PM_{2.5}$, O_3, NO_2, SO_2) in the NCP, the temporal variation of downward shortwave flux at the surface

236   (SWDOWN) in Beijing, Tianjin, Zhengzhou, Hefei and Ji'nan, and the temporal variation of aerosol species (OA,

237   elemental carbon, ammonium, sulphate and nitrite) in Beijing and, Tianjin and of primary OA from BB, RCC,

238   motor vehicles and SOA in Beijing in January, 2014. Detailed data descriptions and quantitative statements of

239   model biases can be found in supplementary text S2.1 and S3. In general, the model simulates reasonably well the

240   air pollutants, SWDOWN, and aerosol species against measurements.

241   SSA determines the strength of aerosols in absorbing solar radiation. Here we conduct three sensitivity

242   experiments to evaluate the effect of BrC with different k values on the simulated aerosol absorption. The first

243   experiment is the control simulation in which all organic aerosols are treated as purely scattering particles with no

244   absorption contribution of BrC, which is referred to as NOBRC. The hi-absorption scenario (HI-BRC-ABS) and

245   low-absorption scenario (LOW-BRC-ABS) characterize BrC light absorption by using the higher and lower

246   imaginary refractive index derived from Section 2.3.2, respectively. Figure 3 shows the comparisons of simulated

247   versus observed SSA at 440 nm (SSA_{440}) at Sun-sky radiometer Observation NETwork (SONET) sites in Beijing,

248   Songshan, Xi'an, Hefei, Nanjing in January 2014. Due to the influence of clouds, the observational data from

249   SONET are not continuous, resulting in a total of 237 valid data points are available for comparison. Moreover,

250   SSA retrieval typically have larger uncertainties at low AOD values (Dubovik et al., 2002). Therefore, we have

251   excluded the SSA data when AOD is less than 0.5, which has 206 valid points in each case. We find that the

252   inclusion of BrC in the model reduces the bias of simulated SSA. The HI-BRC-ABS case demonstrated a largest

253 improvement with the correlation coefficient increasing to 0.54, making it the best simulation in the study. It

254 suggests that stronger BrC absorption case, as prescribed in HI-BRC-ABS, better captures the aerosol optical

255 properties observed in northern China during winter. Consequently, the HI-BRC-ABS case can serve as the the

256 base simulation for further investigation of radiative effects of BrC in this study. Overall, the model tends to

257 underestimate SSA_{440}. The underestimation might be partly caused by the overestimation of absorbing aerosols

258 like BC or dust. Meanwhile, the uncertainties of the simulated SSA can be caused by other factors, such as mixing

259 state of aerosols, particle shape, wavelength, and mass ration of non-black carbon to BC (Liu et al., 2017; Jeong

260 et al., 2020).

261
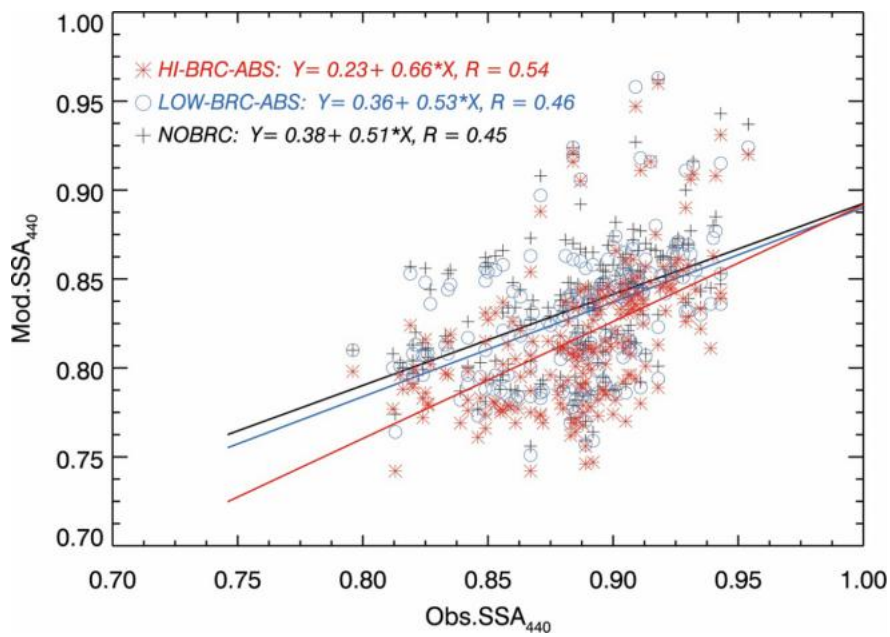
Figure 3. Scatter plot and linear fitting of modelled and observed column integrated SSA at 440 nm in case HI-BRC-ABS (red), LOW-BRC-ABS (blue) and NOBRC (black) case.

264   The daily AOD at 550 nm (AOD_{550}) from the dataset of Long-term Gap-free High-resolution Air Pollutant

265 (LGHAP), derived via tensor-flow-based multimodal data fusion method (Bai et al., 2022), is compared with the

266 simulation. This gap-free daily AOD dataset at 1 km resolution for 2000–2020 in China was generated by

267 integrating multimodal data from satellites, numerical models, and in situ measurements. Data gaps in Moderate

268 Resolution Imaging Spectroradiometer (MODIS) AOD are reconstructed through spatial pattern recognition and

269 statistical knowledge transfer. Validation against Aerosol Robotic Network (AERONET) observations showed

270 strong agreement, with an R of 0.91 and an RMSE of 0.21. Figure 4a and 4b shows the pattern comparison of the

271 monthly simulated and retrieved AOD_{550}. The model reproduces the retrieved AOD distribution in the NCP

272 reasonably. The monthly average simulated and retrieved AOD_{550} is 0.45 and 0.48 on average in the NCP,

273 respectively. Figure 3c shows the scatter plot of the daily simulated and retrieved AOD_{550} averaged in the NCP

274 during the simulation period. The simulated daily average AOD_{550} correlates quite well with the retrieved value,

275 with a regression slope of 1.08 and correlation coefficient of 0.83. Generally, the retrieved and simulated AOD

276 increases with deterioration of the particulate pollution. Figure 5 provides the pattern comparison of the simulated

277 and Ozone Monitoring Instrument (OMI) retrieved AOD at 440 nm (AOD_{440}) averaged during the simulated

278 episode. OMI aboard NASA's Aura satellite offers global atmospheric measurements at a spatial resolution of

279 $0.25° \times 0.25°$, with Beijing's overpass occurring at approximately 13:45 local time. The averaged AOD_{440} from the

280 model simulation at 14:00 local time shows generally agreement with the OMI retrieval. The average simulated

281 and retrieved AOD_{440} is 0.51 and 0.53 in the NCP, respectively. Overall, the model generally performs well in

282 simulating the AOD distribution. It is worth noting that the simulated AOD is not only dependent on the column

283 aerosol content and composition, but is also substantially influenced by relative humidity (RH) which determines

284 the aerosol hygroscopic growth. Additionally, the satellite retrieved AOD is subject to contamination by the

285 presence of clouds, and considering the high occurrence frequency of clouds during haze days, the retrieved AOD

286 might be overestimated (Satheesh et al., 2010; Chand et al., 2012).

287
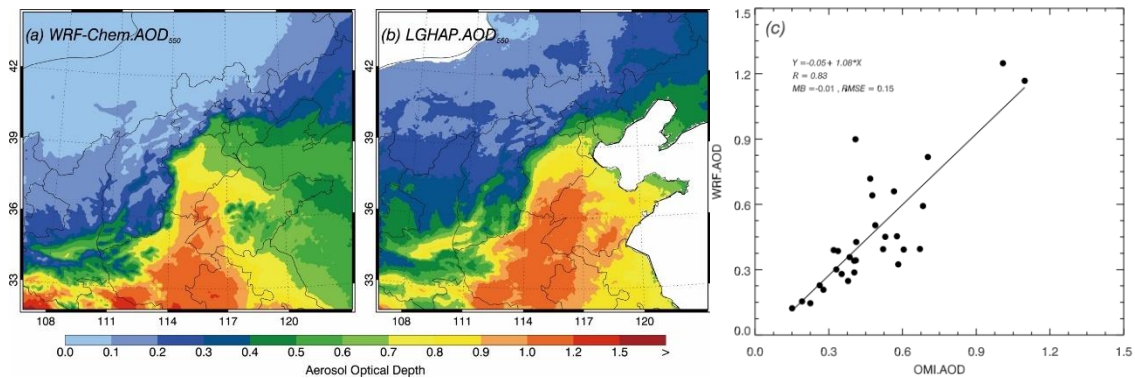
288 **Figure 4 (a) monthly simulated AOD_{550} of WRF-Chem, (b) monthly retrieved AOD_{550} of reanalysis dataset LGHAP,**

289 **and (c) scatter plot of the daily simulated and retrieved AOD_{550} averaged in the NCP from 01 January to 30 January**

290 **2014**

291

292
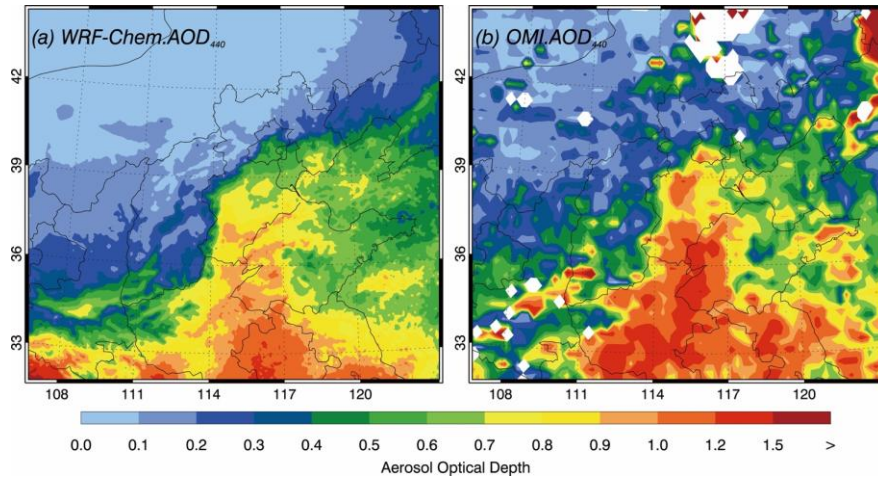
Figure 5 (a) monthly simulated AOD$_{440}$ of WRF-Chem, (b) monthly retrieved AOD$_{440}$ of OMI in the NCP from 01 January to 30 January 2014

3.2 Surface mass concentrations of BrC in NCP

The simulated distribution of average near-surface BrC concentrations and each source contribution in January 2014 is shown in Fig. 6a. In January, the monthly mean concentrations of BrC in the NCP vary from 0.05 μg m^{-3} to 42.3 μg m^{-3}, with an average of 5.2 μg m^{-3}. The spatial distribution of near-surface BrC concentrations is like that of PM$_{2.5}$ in the NCP, with the highest concentration areas located in Hebei Province with an average concentration of 14.9 μg m^{-3}. The simulated BrC concentrations are higher than those reported by Zhu et al.(Bai et al., 2022; Zhu et al., 2021) (2021) in 2018, which is perhaps caused by the more severe particulate pollution in January 2014.
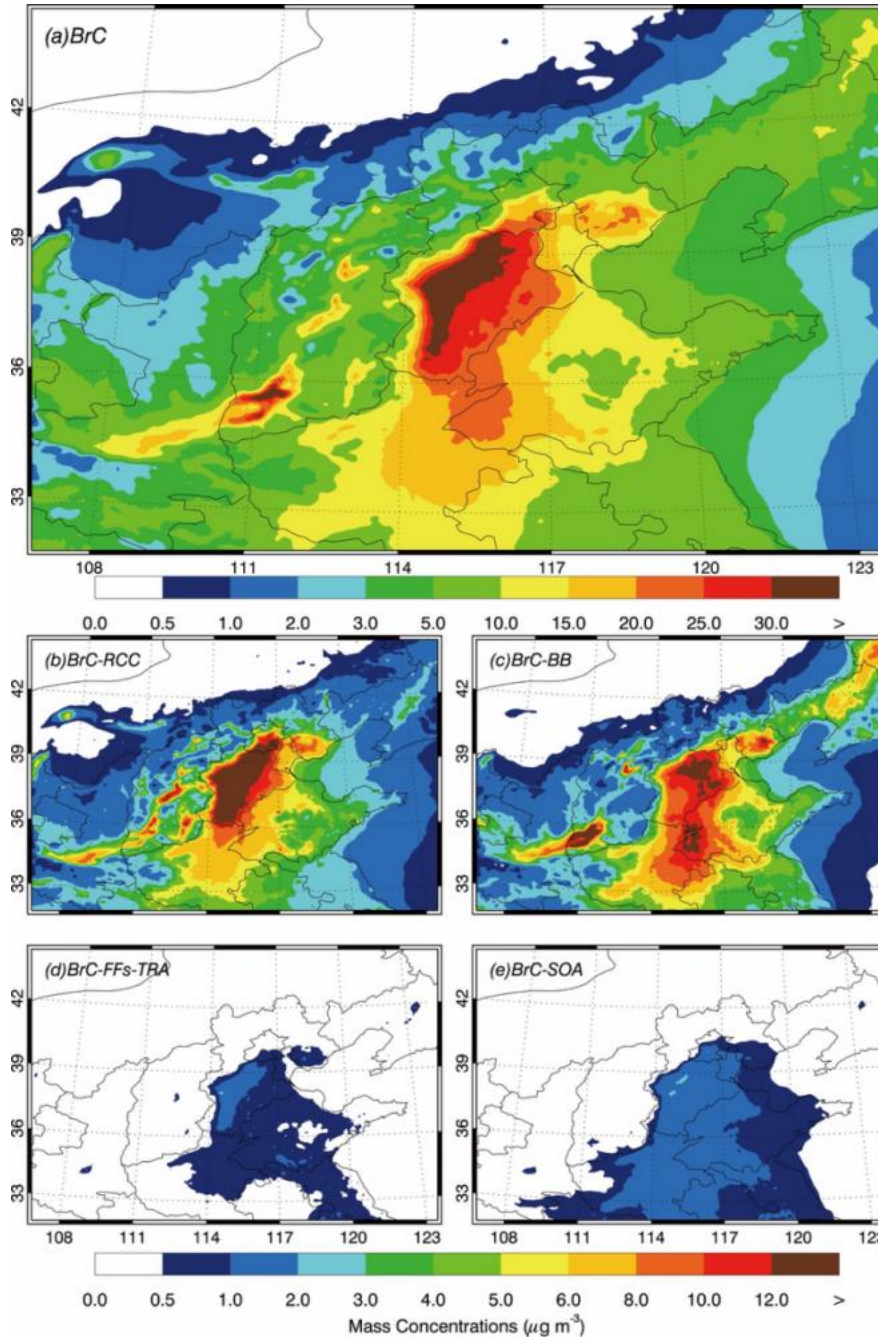
Figure 6. Simulated mean surface concentrations of BrC (a) and contributions from RCC (b), BB (c), FFs-TRA (d) and secondary BrC (e) in January 2014 in NCP

Figure 6b-e present the average near-surface BrC concentrations from different anthropogenic sources and secondary formation in January 2014 in the NCP. The BrC in the NCP predominantly originates from RCC and BB, with an average contribution of 2.3 and 2.4 μg m^{-3} and a maximum of 33.8 and 31.6 μg m^{-3}, respectively. A relatively small proportion of BrC is related to FFs-TRA and secondary transformations with an average concentration of 0.2 μg m^{-3} and 0.4 μg m^{-3}, respectively. The BrC from RCC accounts for 55.8% of total BrC

concentrations in the NCP, which is highest in Beijing, Hebei, and Tianjin, reaching 67.7%, 54.4% and 53.3%

respectively. The BrC from BB counts 36.9% of total BrC concentrations, with a contribution of about 40% in

most provinces of the NCP but only 26.5% in Beijing. This result shows that the RCC is one of the major sources

of BrC in NCP due to the wide use of coal for heating and cooking in winter with low combustion efficiency and

little emission control. The BrC emitted by RCC is mainly concentrated in the Beijing-Tianjin-Hebei (BTH) region

in January 2014, while the BrC emitted by BB is distributed in the whole NCP. The Fen-Wei plain exhibits notably

high contributions from BB, which is consistent with the emission distribution and with previous studies (Cao and

Cui, 2021; Zhang et al., 2021). The Fen-Wei Plain is one of the most densely populated and heavily polluted areas

in northern China where biomass is usually used for heating during winter.

3.3 BrC absorption in the NCP

BrC absorbs visible to near-ultraviolet light with its absorption capabilities extending prominently at shorter

wavelengths. Therefore, we calculate the AAOD (aerosol absorption optical depth) to evaluate the absorption

contribution of BrC versus bulk aerosols, each anthropogenic source and SOA versus BrC at 365 nm (Fig. 7), by

differentiating the AAOD between the model runs with and without the contribution of BrC. The average

contribution of BrC to the total AAOD of aerosols at 365 nm is 16.4% and the maximum is 39.5% in the NCP in

January 2014. The BrC to BC and OC ratios in surface air in the study is 2.2 and 0.31, respectively. They are

higher than the surface ratio used in the global models (Jo et al., 2016; Park et al., 2010), but lower than the ratio

of Feng et al., (2013). Although the concentrations of BrC is relatively high and the absorption of BrC in the

ultraviolet band is comparable to that of BC, the imaginary index of BrC (about 0.1) is still much lower than that

of BC (about 0.76). As a result, the light absorption contribution of BrC at 365 nm is not as significant during the

study period.

Furthermore, the light absorption properties of BrC during the winter season are predominantly attributed to

RCC, followed by BB, SOA, and FFs-TRA in the NCP. The average contribution of RCC and BB to the AAOD

of BrC is 59.3% and 26.3%, respectively. Although the concentration of BrC from RCC is comparable to that

from BB, the much higher light-absorbing property of the BrC from RCC makes it a dominant contributor to the

overall light absorption caused by BrC. Despite lower surface concentrations compared to primary BrC,

secondary BrC contributes significantly to AAOD of BrC, averaging ~10.0% with elevated contributions in

the sea and remote regions, which is likely due to the highly oxidized character of organic aerosols and its

chemical aging in aging air masses leading to the formation of BrC (Gouw et al., 2005; Kawamura et al.,

340   2005; Tsigaridis and Kanakidou, 2018). While AOD represents column-integrated concentrations, the

341   secondary BrC to Primary BrC ratio increases from 8.9% at the surface to 12.0% of atmospheric burden. It

342   reaches 14.3% at an altitude of 500m as shown in Figure S6, which could lead to a higher absorption

343   contribution of secondary BrC (Wang et al., 2022b). Moreover, the observations indicate that a substantial

344   SOA is water-soluble (Maria et al., 2003; Peng et al., 2021) which is treated as hygroscopic components in

345   the model and its absorption could be magnified. The AAOD contribution of BrC from vehicles is the lowest,

346   about 1.8% on average, but its contribution in southern Jiangsu and southeast Anhui ranges from 4% to 8%, higher

347   than in other regions. This may suggest that motor vehicle emissions account for a significant proportion of

348   pollution in this area.

349
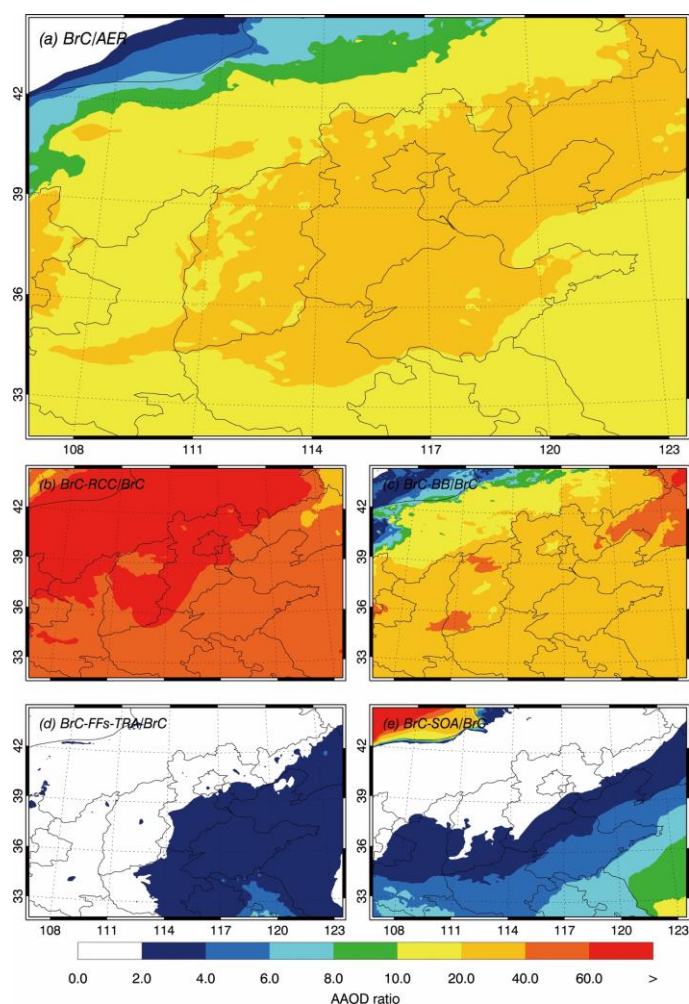
350   **Figure 7 Simulated monthly BrC AAOD versus aerosol at 365nm (a) and each anthropogenic source of RCC (b), BB(c),**

351   **FFs-TRA (d) and secondary BrC (d) AAOD versus BrC in NCP**

3.4 Direct radiative effect of BrC

Figure. 8a shows the distribution of the average DRE_{TOA} caused by BrC at the top of the atmosphere during the episode. The DRE_{TOA} of BrC in the NCP is -0.09 W m^{-2} on average, with a maximum of +0.46 W m^{-2} and a minimum of -2.74 W m^{-2}. Compared to the average DRE_{TOA} of BC +3.9 W m^{-2} and a maximum of +21.6 W m^{-2}, the average DRE_{TOA} of BrC in the NCP is close to zero. However, in terms of the spatial distribution, the DRE_{TOA} of total BrC in the NCP is predominantly negative, especially in those areas with high BrC concentrations including BTH area and Fen-wei Plain. The largest negative DRE_{TOA} is in Shanxi province, where the highest contributor to BrC is BB. The overall scattering effect of BrC is greater than its absorption effect, so that BrC have a net cooling effect. The solar irradiance in the UV band contributes only 10% of the total solar irradiation and the imaginary refractive indices of BrC are much lower than those strongly absorbing BC, especially in the visible band. On the other hand, although this leads to a small heating effect by BrC, the increased DRE_{TOA} induced by BrC which is usually considered as its scattering effect, is up to an average of +0.40 W m^{-2} and a maximum of +1.83 W m^{-2} as shown in Fig. 8b. The DRE_{TOA} of OA without BrC is -2.00 W m^{-2} over the NCP (Fig. 8d) and is increased to -1.60 W m^{-2} (Fig. 8c) after considering BrC. Consequently, the cooling effect of OA is reduced by BrC by an average of 28.0%. So far, almost all estimates of the radiation effects of BrC have been based on a global basis. The study of Wang et al. (2014) reported a global DRE_{TOA} of BrC of -0.02 W m^{-2}, resulting in a DRE_{TOA} increase of +0.07 W m^{-2}. Brown et al. (2018) have also reported a global annual increased DRE_{TOA} of +0.13 W m^{-2}, with the maximum forcing (~+1.75 W m^{-2}) occurring at the west coast of southern Africa. BrC reduces the cooling effect caused by organic aerosols by approximately 16% (Jo et al., 2016). However, all these estimates only considered BB, biofuels or SOA and the significance of BrC in the estimates for these studies typically based on the assumption that OA primarily scatters sun light. Our results indicate that the solar radiation changes caused by BrC in NCP is notable. The absorption effect of BrC should be considered in climate models to accurately assess the aerosol impact on atmospheric heating and climate change.
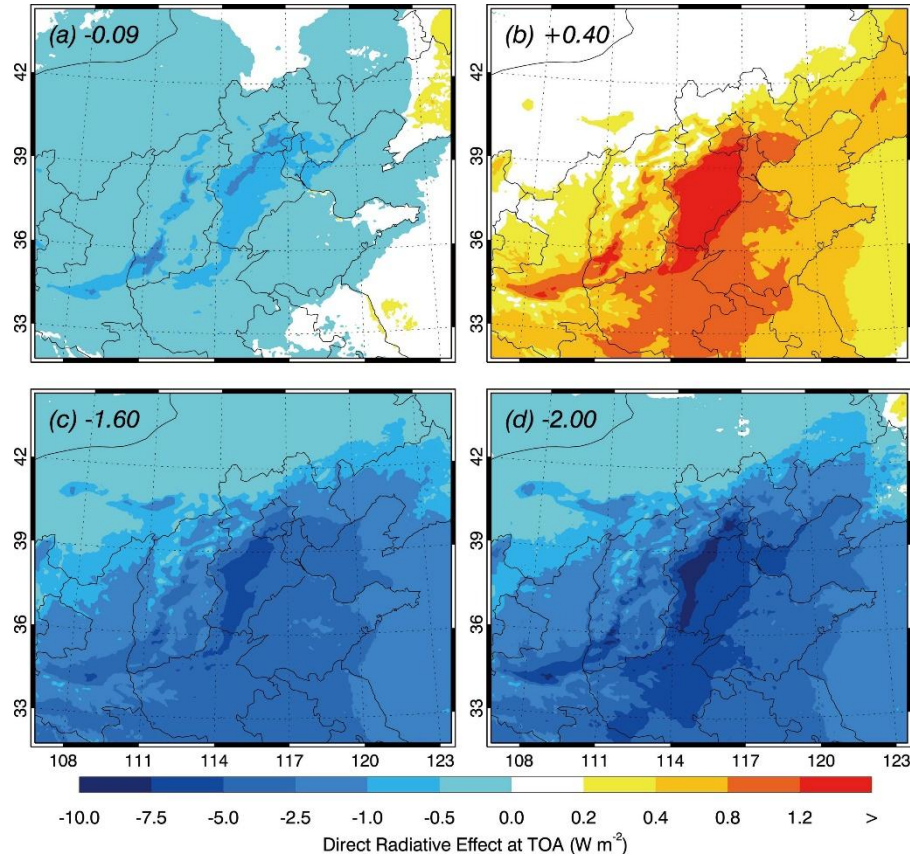
Figure 8, Estimated DRE$_{TOA}$ of BrC (a) and DRE$_{TOA}$ increase of OA owing to the absorption of BrC (b). The DRE$_{TOA}$ of total OA with absorbing BrC (c) and DRE$_{TOA}$ of total OA with BrC is assumed to be scattering (d). The averages of DRE are shown in the upper left of each panel.

Figure 9a-d shows the estimated DRE$_{TOA}$ of BrC from RCC, BB, FFs-TRA and secondary BrC in the NCP during the episode. Similar to the contribution of BrC sources to the AAOD at 365 nm, the most important source contributing to DRE$_{TOA}$ of BrC is RCC (+0.26 W m^{-2}), followed by BB (+0.11 W m^{-2}), secondary BrC (+0.02 W m^{-2}), and FFs-TRA (+0.01 W m^{-2}) in the NCP, as shown in Fig. 9. In addition, the DRE$_{TOA}$ of BrC from various sources exhibits distinct spatial distribution characteristics in the NCP. The highest DRE$_{TOA}$ of BrC from fossil sources, which include RCC and FFs-TRA, are predominantly concentrated in Hebei. The highest positive DRE$_{TOA}$ of BrC from BB is found in Fen-Wei Plain. Meanwhile, the secondary BrC contributes most to the DRE$_{TOA}$ in the south part of the NCP. The persistent high values over southern China might stem from the model's representation of secondary BrC as hygroscopic components (Peng et al., 2021), whose light-absorbing capacity is amplified in the region with high ambient humidity.
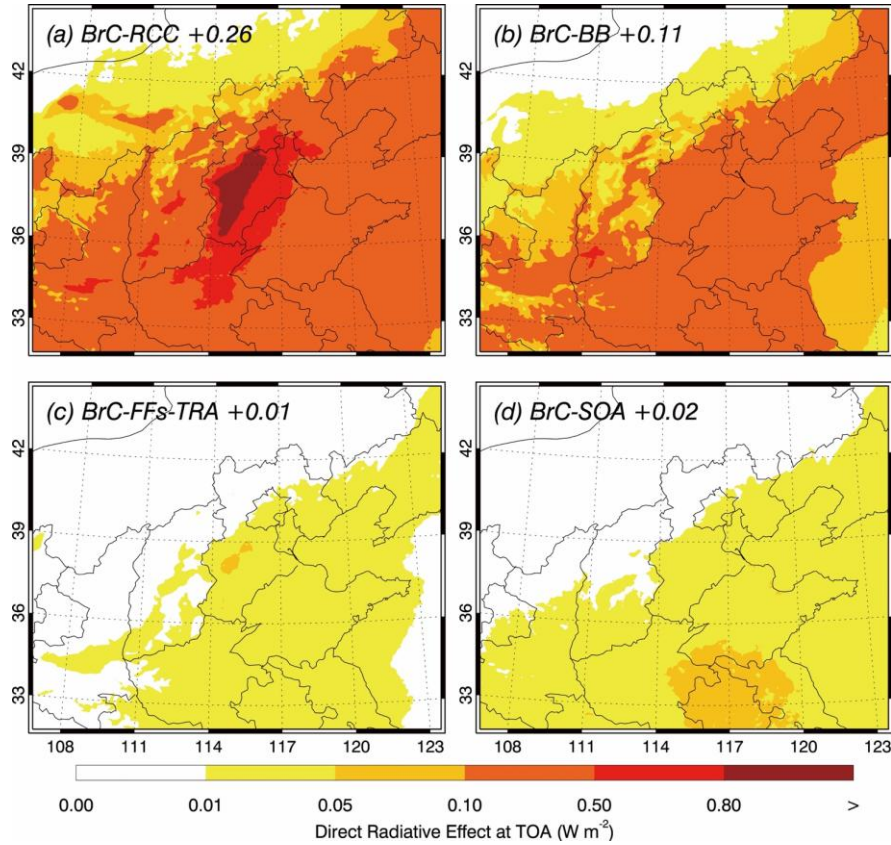
Figure 9. The estimation DRE_TOA of BrC from each anthropogenic source RCC(a), BB(b), FFs-TRA(c) and secondary BrC(d) in NCP in January 2014

4 Conclusions

A source-explicit BrC simulation in January 2014 in the NCP is conducted by using the WRF-Chem model. We define the BrC based on varying proportions of RCC, BB, FFs-TRA and SOA sources, assigning each a distinct imaginary refractive index to represent their differing light absorption characteristics. Model simulations are evaluated with various data sets. Besides the well reproduction of temporal and spatial variations of aerosol components and SWDOWN in the model, AOD and SSA are used to evaluate the aerosol optical properties.

Near-surface mass concentrations of simulated BrC in the NCP range from 0.05 to 42.3 $\mu g\ m^{-3}$ with an average of 5.2 $\mu g\ m^{-3}$, which is mainly attributed to RCC and BB, especially in the BTH region and Fen-Wei Plain. Estimation of the BrC contribution to AAOD shows that the BrC accounts for an average of 16.4% and up to 39.5% of the total aerosol absorption at 365 nm. The largest contributor to the absorption of BrC is RCC derived BrC, reaching 59.3%. BrC generally has a net cooling effect in the NCP if we consider both the absorption and scattering properties, with DRE_TOA of BrC of around -0.09 W m^{-2} on average and ranging between -2.74 W m^{-2} and +0.46

404   W m^{-2}. However, the absorption of BrC increases the DRE$_{TOA}$ of OA by 28.0% with an average of +0.40 W m^{-2}

405   and a maximum of +1.83 W m^{-2}. The average increase in DRE$_{TOA}$ of BrC from RCC, BB, secondary formation,

406   and FFs-TRA is +0.26 W m^{-2}, +0.11 W m^{-2}, +0.02 W m^{-2}, +0.01 W m^{-2}, respectively. Our results indicate that BrC

407   derived from RCC may have significant implications for regions relying heavily on coal as their primary energy

408   source, such as northern China. Climate models should not only incorporate the absorption of BrC but also account

409   for residential coal burning as a potentially important BrC emission source. Additionally, although we conducted

410   simulations with a relatively conservative secondary BrC, the impact of secondary BrC on radiative processes

411   should not be overlooked. More field observation and model experiments should be carried out in the future for

412   better understanding of its role in atmospheric radiation balance.

413   It should be noted that China has started to switch from coal to cleaner and more efficient energy such as

414   natural gas or liquid petroleum gas in recent years. According to the latest report of National Bureau of Statistics

415   of China, the total coal consumption for residential use was 55.5 Gg in 2022 (https://data.stats.gov.cn)with a

416   40.3% decrease compared to 2014. Therefore, our diagnosis of the sources of BrC and their radiative effects is

417   specifically targeted at the winter season in 2014. Moreover, future simulations should strengthen the

418   parameterization for the evolution of BrC, such as bleaching or darkening processes.

419   The simulation of BrC in climate models is fraught with uncertainties due to its diverse sources which result

420   in a wide range of optical properties. The absorption characteristics of BrC can change significantly as it undergoes

421   atmospheric aging, impacting its radiative forcing estimates. Additionally, interactions of BrC with other

422   atmospheric particles and its effects on cloud microphysics and albedo introduce further complexities in modeling

423   its climate impact. These uncertainties necessitate enhanced observational data and better integration of BrC

424   properties in climate models to improve the accuracy of climate predictions and assessments. Although the

425   simulations have been evaluated with extensive aerosol mass and optical measurements, more field measurements

426   and lab experiments are needed, especially for the inventory development of BrC, the vertical profiles from

427   aircrafts, and physicochemical properties which would be useful for further evaluating and improving model

428   performance.

429   **Author contributions**

430   Guohui Li and Xuexi Tie designed the study. Jiamao Zhou and Guohui Li wrote the paper. Jiamao Zhou,

431   Jiarui Wu, Xi Li, Ruonan Wang performed the model simulations. Xiaoli Su and Jiang Qian collected satellites

432 and ground-based observation data. Ting Zhang, Wenting Dai and Junji Cao performed field observation and

433 laboratory analysis. Imad EI Haddad and Andre S.H. Prevot provided the data of OA components in Beijing,

434 kindly reviewed the language writing of the manuscript and provided some supplementary suggestions for the

435 paper. All authors reviewed and commented on the paper.

436 **Acknowledgments**

437 This work was financially supported by the project of Yong Scientists Fund of the National Natural Science

438 Foundation of China (42107127).

439 **Data availability**

440 The Chinese Ecosystem Research Network (CERN) provided the radiation observation data. The AOD_{550}

441 data is supported from "National Earth System Science Data Center (https://www.geodata.cn)" and AOD_{440}

442 provided by OMI Science Team (https://www.earthdata.nasa.gov/learn/find-data/near-real-time/omi). The SSA

443 data is supported by Sun-sky Radiometer Observation NETwork (http://www.sonet.ac.cn) and the historic profiles

444 of the observed ambient air pollutants provided by Ministry of Ecology and Environment of China

445 (https://www.aqistudy.cn/).

446 **Competing interests**

447 The authors declare that they have no conflict of interest.

448

References

Andreae, M. O. and Gelencsér, A.: Black carbon or brown carbon?: The nature of light-absorbing carbonaceous aerosols, Atmos. Chem. Phys., 6, 3131–3148, https://doi.org/10.5194/acp-6-3131-2006, 2006.

Bai, K., Li, K., Ma, M., Li, K., Li, Z., Guo, J., Chang, N.-B., Tan, Z., and Di Han: LGHAP: the Long-term Gap-free High-resolution Air Pollutant concentration dataset, derived via tensor-flow-based multimodal data fusion, Earth Syst. Sci. Data, 14, 907–927, https://doi.org/10.5194/essd-14-907-2022, 2022.

Bohren, C. F. and Huffman, D. R.: Absorption and Scattering of Light by Small Particles, Wiley, 1998.

Bond, T. C., Doherty, S. J., Fahey, D. W., Forster, P. M., Berntsen, T., DeAngelo, B. J., Flanner, M. G., Ghan, S., Kärcher, B., Koch, D., Kinne, S., Kondo, Y., Quinn, P. K., Sarofim, M. C., Schultz, M. G., Schulz, M., Venkataraman, C., Zhang, H., Zhang, S., Bellouin, N., Guttikunda, S. K., Hopke, P. K., Jacobson, M. Z., Kaiser, J. W., Klimont, Z., Lohmann, U., Schwarz, J. P., Shindell, D., Storelvmo, T., Warren, S. G., and Zender, C. S.: Bounding the role of black carbon in the climate system: A scientific assessment, J. Geophys. Res., 118, 5380–5552, https://doi.org/10.1002/jgrd.50171, 2013.

Bond, T. C.: Spectral dependence of visible light absorption by carbonaceous particles emitted from coal combustion, Geophys. Res. Lett., 28, 4075–4078, https://doi.org/10.1029/2001GL013652, 2001.

Brown, H., Liu, X., Feng, Y., Jiang, Y., Wu, M., Lu, Z., Wu, C., Murphy, S., and Pokhrel, R.: Radiative effect and climate impacts of brown carbon with the Community Atmosphere Model (CAM5), Atmos. Chem. Phys., 18, 17745–17768, https://doi.org/10.5194/acp-18-17745-2018, 2018.

Browne, E. C., Zhang, X., Franklin, J. P., Ridley, K. J., Kirchstetter, T. W., Wilson, K. R., Cappa, C. D., and Kroll, J. H.: Effect of heterogeneous oxidative aging on light absorption by biomass burning organic aerosol, Aerosol Science and Technology, 53, 663–674, https://doi.org/10.1080/02786826.2019.1599321, 2019.

Cao, J. J. and Cui, L.: Current Status, Characteristics and Causes of Particulate Air Pollution in the Fenwei Plain, China: A Review, J. Geophys. Res., 126, https://doi.org/10.1029/2020JD034472, 2021.

Chakrabarty, R. K., Moosmüller, H., Chen, L.-W. A., Lewis, K., Arnott, W. P., Mazzoleni, C., Dubey, M. K., Wold, C. E., Hao, W. M., and Kreidenweis, S. M.: Brown carbon in tar balls from smoldering biomass combustion, Atmos. Chem. Phys., 10, 6363–6370, https://doi.org/10.5194/acp-10-6363-2010, 2010.

Chen, W., Wang, Z., Zhao, H., and Qin, K.: A novel way to calculate shortwave black carbon direct radiative effect, The Science of the total environment, 756, 142961, https://doi.org/10.1016/j.scitotenv.2020.142961, 2021.

Chen, Y. and Bond, T. C.: Light absorption by organic carbon from wood combustion, Atmos. Chem. Phys., 10,

478 1773–1787, https://doi.org/10.5194/acp-10-1773-2010, 2010.

479 Cheng, Z., Atwi, K. M., Yu, Z., Avery, A., Fortner, E. C., Williams, L., Majluf, F., Krechmer, J. E., Lambe, A. T.,

480 and Saleh, R.: Evolution of the light-absorption properties of combustion brown carbon aerosols following

481 reaction with nitrate radicals, Aerosol Science and Technology, 54, 849–863,

482 https://doi.org/10.1080/02786826.2020.1726867, 2020.

483 Corbin, J. C., Czech, H., Massabò, D., Mongeot, F. B. de, Jakobi, G., Liu, F., Lobo, P., Mennucci, C., Mensah, A.

484 A., Orasche, J., Pieber, S. M., Prévôt, A. S. H., Stengel, B., Tay, L.-L., Zanatta, M., Zimmermann, R., El Haddad,

485 I., and Gysel, M.: Infrared-absorbing carbonaceous tar can dominate light absorption by marine-engine exhaust,

486 npj Clim Atmos Sci, 2, 3985, https://doi.org/10.1038/s41612-019-0069-5, 2019.

487 D'Almeida, G.A., Koepke, P. and Shettle, E.P.: Atmospheric Aerosols: Global Climatology and Radiative

488 Characteristics, A.Deepak Publ, Hampton, Virginia, 1991.

489 Dubovik, O., Holben, B., Eck, T. F., Smirnov, A., Kaufman, Y. J., King, M. D., Tanré, D., and Slutsker, I.:

490 Variability of Absorption and Optical Properties of Key Aerosol Types Observed in Worldwide Locations, J.

491 Atmos. Sci., 59, 590–608, https://doi.org/10.1175/1520-0469(2002)059<0590:VOAAOP>2.0.CO;2, 2002.

492 Fast, J. D., Gustafson, W. I., Easter, R. C., Zaveri, R. A., Barnard, J. C., Chapman, E. G., Grell, G. A., and Peckham,

493 S. E.: Evolution of ozone, particulates, and aerosol direct radiative forcing in the vicinity of Houston using a fully

494 coupled meteorology-chemistry-aerosol model, J. Geophys. Res., 111, 2981,

495 https://doi.org/10.1029/2005JD006721, 2006.

496 Feng, Y., Ramanathan, V., and Kotamarthi, V. R.: Brown carbon: A significant atmospheric absorber of solar

497 radiation?, Atmos. Chem. Phys., 13, 8607–8621, 2013.

498 Forrister, H., Liu, J., Scheuer, E., Dibb, J., Ziemba, L., Thornhill, K. L., Anderson, B., Diskin, G., Perring, A. E.,

499 Schwarz, J. P., Campuzano-Jost, P., Day, D. A., Palm, B. B., Jimenez, J. L., Nenes, A., and Weber, R. J.: Evolution

500 of brown carbon in wildfire plumes, Geophys. Res. Lett., 42, 4623–4630, https://doi.org/10.1002/2015GL063897,

501 2015.

502 Fountoukis, C. and Nenes, A.: ISORROPIA II: a computationally efficient thermodynamic equilibrium model for

503 $K^+–Ca^{2+}–Mg^{2+}–NH_4^+–Na^+–SO_4^{2-}–NO_3^-–Cl^-–H_2O$ aerosols, Atmos. Chem. Phys., 7, 4639–4659,

504 https://doi.org/10.5194/acp-7-4639-2007, 2007.

505 Gao, Y., Gao, P., Zhuang, B., Hu, Y., Zhou, Y., Wang, T., Li, S., Li, M., and Xie, M.: Changes in the Climate

506 Effects of Major Anthropogenic Aerosols in East Asia Under Different Emission Reduction Scenarios in China, J.

507   Geophys. Res., 130, https://doi.org/10.1029/2024JD042301, 2025.

508   Ge, W., Prime, N. S., Smith, S. J., Liu, J., Ren, Y., Zhou, Y., Wu, H., Wang, X., and Chen, G.: The short-term

509   comprehensive impact of the phase-out of global coal combustion on air pollution and climate change,

510   Environmental pollution (Barking, Essex 1987), 367, 125669, https://doi.org/10.1016/j.envpol.2025.125669,

511   2025.

512   Gouw, J. A. de, Middlebrook, A. M., Warneke, C., Goldan, P. D., Kuster, W. C., Roberts, J. M., Fehsenfeld, F. C.,

513   Worsnop, D. R., Canagaratna, M. R., Pszenny, A. A. P., Keene, W. C., Marchewka, M., Bertman, S. B., and Bates,

514   T. S.: Budget of organic carbon in a polluted atmosphere: Results from the New England Air Quality Study in

515   2002, J. Geophys. Res., 110, https://doi.org/10.1029/2004JD005623, 2005.

516   Grell, G. A., Peckham, S. E., Schmitz, R., McKeen, S. A., Frost, G., Skamarock, W. C., and Eder, B.: Fully coupled

517   "online"   chemistry   within   the   WRF   model,   Atmospheric   Environment,   39,   6957–6975,

518   https://doi.org/10.1016/j.atmosenv.2005.04.027, 2005.

519   Guenther, A., Karl, T., Harley, P., Wiedinmyer, C., Palmer, P. I., and Geron, C.: Estimates of global terrestrial

520   isoprene emissions using MEGAN (Model of Emissions of Gases and Aerosols from Nature), Atmos. Chem. Phys.,

521   6, 3181–3210, https://doi.org/10.5194/acp-6-3181-2006, 2006.

522   Hammer, M. S., Martin, R. V., van Donkelaar, A., Buchard, V., Torres, O., Ridley, D. A., and Spurr, R. J. D.:

523   Interpreting the ultraviolet aerosol index observed with the OMI satellite instrument to understand absorption by

524   organic aerosols: Implications for atmospheric oxidation and direct radiative effects, Atmos. Chem. Phys., 16,

525   2507–2523, https://doi.org/10.5194/acp-16-2507-2016, 2016.

526   Hecobian, A., Zhang, X., Zheng, M., Frank, N., Edgerton, E. S., and Weber, R. J.: Water-Soluble Organic Aerosol

527   material and the light-absorption characteristics of aqueous extracts measured over the Southeastern United States,

528   Atmos. Chem. Phys., 10, 5965–5977, https://doi.org/10.5194/acp-10-5965-2010, 2010.

529   Hoffer, A., Gelencsér, A., Guyon, P., Kiss, G., Schmid, O., Frank, G. P., Artaxo, P., and Andreae, M. O.: Optical

530   properties of humic-like substances (HULIS) in biomass-burning aerosols, Atmos. Chem. Phys., 6, 3563–3570,

531   https://doi.org/10.5194/acp-6-3563-2006, 2006.

532   Huang, R.-j., Yuan, W., Yang, L., Yang, H., Cao, W., Guo, J., Zhang, N., Zhu, C., Wu, Y., and Zhang, R.:

533   Concentration, optical characteristics, and emission factors of brown carbon emitted by on-road vehicles, The

534   Science of the total environment, 810, 151307, https://doi.org/10.1016/j.scitotenv.2021.151307, 2022.

535   Huang, X., Song, Y., Zhao, C., Cai, X., Zhang, H., and Zhu, T.: Direct Radiative Effect by Multicomponent

Aerosol over China*, Journal of Climate, 28, 3472–3495, https://doi.org/10.1175/JCLI-D-14-00365.1, 2015.

Hurley, M. D., Sokolov, O., Wallington, T. J., Takekawa, H., Karasawa, M., Klotz, B., Barnes, I., and Becker, K. H.: Organic aerosol formation during the atmospheric degradation of toluene, Environmental science & technology, 35, 1358–1366, https://doi.org/10.1021/es0013733, 2001.

IPCC (Ed.): Climate Change 2013: The Physical Science Basis. Contribution of Working Group I to the Fifth Assessment Report of the Intergovernmental Panel on Climate Change, Cambridge University Press, Cambridge, United Kingdom and New York, NY, USA, 2013.

Jacobson, M. Z.: Effects of biomass burning on climate, accounting for heat and moisture fluxes, black and brown carbon, and cloud absorption effects, J. Geophys. Res., 119, 8980–9002, https://doi.org/10.1002/2014JD021861, 2014.

Jacobson, M. Z.: Isolating nitrated and aromatic aerosols and nitrated aromatic gases as sources of ultraviolet light absorption, J. Geophys. Res., 104, 3527–3542, https://doi.org/10.1029/1998JD100054, 1999.

Jeong, J. I., Jo, D. S., Park, R. J., Lee, H.-M., Curci, G., and Kim, S.-W.: Parametric analysis for global single scattering albedo calculations, Atmospheric Environment, 234, 117616, https://doi.org/10.1016/j.atmosenv.2020.117616, 2020.

Jo, D. S., Nault, B. A., Tilmes, S., Gettelman, A., McCluskey, C. S., Hodzic, A., Henze, D. K., Nawaz, M. O., Fung, K. M., and Jimenez, J. L.: Global Health and Climate Effects of Organic Aerosols from Different Sources, Environmental science & technology, 57, 13793–13807, https://doi.org/10.1021/acs.est.3c02823, 2023.

Jo, D. S., Park, R. J., Lee, S., Kim, S.-W., and Zhang, X.: A global simulation of brown carbon: Implications for photochemistry and direct radiative effect, Atmos. Chem. Phys., 16, 3413–3432, https://doi.org/10.5194/acp-16-3413-2016, 2016.

Kawamura, K., Imai, Y., and Barrie, L. A.: Photochemical production and loss of organic acids in high Arctic aerosols during long-range transport and polar sunrise ozone depletion events, Atmospheric Environment, 39, 599–614, https://doi.org/10.1016/j.atmosenv.2004.10.020, 2005.

Kirchstetter, T. W., Novakov, T., and Hobbs, P. V.: Evidence that the spectral dependence of light absorption by aerosols is affected by organic carbon, J. Geophys. Res., 109, n/a-n/a, https://doi.org/10.1029/2004JD004999, 2004.

Kumar, N. K., Corbin, J. C., Bruns, E. A., Massabó, D., Slowik, J. G., Drinovec, L., Močnik, G., Prati, P., Vlachou, A., Baltensperger, U., Gysel, M., El-Haddad, I., and Prévôt, A. S. H.: Production of particulate brown carbon

during atmospheric aging of residential wood-burning emissions, Atmos. Chem. Phys., 18, 17843–17861, https://doi.org/10.5194/acp-18-17843-2018, 2018.

Lack, D. A., Langridge, J. M., Bahreini, R., Cappa, C. D., Middlebrook, A. M., and Schwarz, J. P.: Brown carbon and internal mixing in biomass burning particles, Proceedings of the National Academy of Sciences of the United States of America, 109, 14802–14807, https://doi.org/10.1073/pnas.1206575109, 2012.

Laskin, A., Laskin, J., and Nizkorodov, S. A.: Chemistry of atmospheric brown carbon, Chemical reviews, 115, 4335–4382, https://doi.org/10.1021/cr5006167, 2015.

Li, C., He, Q., Hettiyadura, A. P. S., Käfer, U., Shmul, G., Meidan, D., Zimmermann, R., Brown, S. S., George, C., Laskin, A., and Rudich, Y.: Formation of Secondary Brown Carbon in Biomass Burning Aerosol Proxies through NO3 Radical Reactions, Environmental science & technology, 54, 1395–1405, https://doi.org/10.1021/acs.est.9b05641, 2020.

Li, G., Lei, W., Bei, N., and Molina, L. T.: Contribution of garbage burning to chloride and $PM_{2.5}$ in Mexico City, Atmos. Chem. Phys., 12, 8751–8761, https://doi.org/10.5194/acp-12-8751-2012, 2012.

Li, G., Bei, N., Tie, X., and Molina, L. T.: Aerosol effects on the photochemistry in Mexico City during MCMA-2006/MILAGRO campaign, Atmos. Chem. Phys., 11, 5169–5182, https://doi.org/10.5194/acp-11-5169-2011, 2011a.

Li, G., Zavala, M., Lei, W., Tsimpidi, A. P., Karydis, V. A., Pandis, S. N., Canagaratna, M. R., and Molina, L. T.: Simulations of organic aerosol concentrations in Mexico City using the WRF-CHEM model during the MCMA-2006/MILAGRO campaign, Atmos. Chem. Phys., 11, 3789–3809, https://doi.org/10.5194/acp-11-3789-2011, 2011b.

Li, G., Lei, W., Zavala, M., Volkamer, R., Dusanter, S., Stevens, P., and Molina, L. T.: Impacts of HONO sources on the photochemistry in Mexico City during the MCMA-2006/MILAGO Campaign, Atmos. Chem. Phys., 10, 6551–6567, https://doi.org/10.5194/acp-10-6551-2010, 2010.

Li, M., Fan, X., Zhu, M., Zou, C., Song, J., Wei, S., Jia, W., and Peng, P.'a.: Abundance and Light Absorption Properties of Brown Carbon Emitted from Residential Coal Combustion in China, Environmental science & technology, 53, 595–603, https://doi.org/10.1021/acs.est.8b05630, 2019.

Li, M., Liu, H., Geng, G., Hong, C., Liu, F., Song, Y., Tong, D., Zheng, B., Cui, H., Man, H., Zhang, Q., and He, K.: Anthropogenic emission inventories in China: a review, National Science Review, 4, 834–866, https://doi.org/10.1093/nsr/nwx150, 2017.

594 Li, X., Wu, J., Elser, M., Feng, T., Cao, J., El-Haddad, I., Huang, R., Tie, X., Prévôt, A. S. H., and Li, G.:

595 Contributions of residential coal combustion to the air quality in Beijing–Tianjin–Hebei (BTH), China: a case

596 study, Atmos. Chem. Phys., 18, 10675–10691, https://doi.org/10.5194/acp-18-10675-2018, 2018.

597 Lin, G., Penner, J. E., Flanner, M. G., Sillman, S., Xu, L., and Zhou, C.: Radiative forcing of organic aerosol in

598 the atmosphere and on snow: Effects of SOA and brown carbon, J. Geophys. Res., 119, 7453–7476,

599 https://doi.org/10.1002/2013JD021186, 2014.

600 Lin, P., Bluvshtein, N., Rudich, Y., Nizkorodov, S. A., Laskin, J., and Laskin, A.: Molecular Chemistry of

601 Atmospheric Brown Carbon Inferred from a Nationwide Biomass Burning Event, Environmental science &

602 technology, 51, 11561–11570, https://doi.org/10.1021/acs.est.7b02276, 2017.

603 Liu, D., Whitehead, J., Alfarra, M. R., Reyes-Villegas, E., Spracklen, D. V., Reddington, C. L., Kong, S., Williams,

604 P. I., Ting, Y.-C., Haslett, S., Taylor, J. W., Flynn, M. J., Morgan, W. T., McFiggans, G., Coe, H., and Allan, J. D.:

605 Black-carbon absorption enhancement in the atmosphere determined by particle mixing state, Nature Geosci, 10,

606 184–188, https://doi.org/10.1038/ngeo2901, 2017.

607 Liu, J., Bergin, M., Guo, H., King, L., Kotra, N., Edgerton, E., and Weber, R. J.: Size-resolved measurements of

608 brown carbon in water and methanol extracts and estimates of their contribution to ambient fine-particle light

609 absorption, Atmos. Chem. Phys., 13, 12389–12404, https://doi.org/10.5194/acp-13-12389-2013, 2013.

610 Lu, Z., Streets, D. G., Winijkul, E., Yan, F., Chen, Y., Bond, T. C., Feng, Y., Dubey, M. K., Liu, S., Pinto, J. P., and

611 Carmichael, G. R.: Light absorption properties and radiative effects of primary organic aerosol emissions,

612 Environmental science & technology, 49, 4868–4877, https://doi.org/10.1021/acs.est.5b00211, 2015.

613 Ma, Y., Jin, Y., Zhang, M., Gong, W., Hong, J., Jin, S., Shi, Y., Zhang, Y., and Liu, B.: Aerosol optical properties

614 of haze episodes in eastern China based on remote-sensing observations and WRF-Chem simulations, The Science

615 of the total environment, 757, 143784, https://doi.org/10.1016/j.scitotenv.2020.143784, 2021.

616 Maria, S. F., Russell, L. M., Turpin, B. J., Porcja, R. J., Campos, T. L., Weber, R. J., and Huebert, B. J.: Source

617 signatures of carbon monoxide and organic functional groups in Asian Pacific Regional Aerosol Characterization

618 Experiment (ACE-Asia) submicron aerosol types, J. Geophys. Res., 108, 295,

619 https://doi.org/10.1029/2003JD003703, 2003.

620 Mo, Y., Li, J., Cheng, Z., Zhong, G., Zhu, S., Tian, C., Chen, Y., and Zhang, G.: Dual Carbon Isotope-Based

621 Source Apportionment and Light Absorption Properties of Water-Soluble Organic Carbon in PM 2.5 Over China,

622 J. Geophys. Res., 126, 27805, https://doi.org/10.1029/2020JD033920, 2021.

Moise, T., Flores, J. M., and Rudich, Y.: Optical properties of secondary organic aerosols and their changes by chemical processes, Chemical reviews, 115, 4400–4439, https://doi.org/10.1021/cr5005259, 2015.

Mukai, H. and Ambe, Y.: Characterization of a humic acid-like brown substance in airborne particulate matter and tentative identification of its origin, Atmospheric Environment (1967), 20, 813–819, https://doi.org/10.1016/0004-6981(86)90265-9, 1986.

Nenes, A., Pandis, S. N., and Pilinis Christodoulos: ISORROPIA: A New Thermodynamic Equilibrium Model for Multiphase Multicomponent Inorganic Aerosols, Aquatic Geochemistry, 4, 123–152, 1998.

Ni, H., Huang, R.-j., Pieber, S. M., Corbin, J. C., Stefenelli, G., Pospisilova, V., Klein, F., Gysel-Beer, M., Yang, L., Baltensperger, U., Haddad, I. E., Slowik, J. G., Cao, J., Prévôt, A. S. H., and Dusek, U.: Brown Carbon in Primary and Aged Coal Combustion Emission, Environmental science & technology, 55, 5701–5710, https://doi.org/10.1021/acs.est.0c08084, 2021.

Park, R. J., Kim, M. J., Jeong, J. I., Youn, D., and Kim, S.: A contribution of brown carbon aerosol to the aerosol light absorption and its radiative forcing in East Asia, Atmospheric Environment, 44, 1414–1421, https://doi.org/10.1016/j.atmosenv.2010.01.042, 2010.

Peng, C., Razafindrambinina, P. N., Malek, K. A., Chen, L., Wang, W., Huang, R.-j., Zhang, Y., Ding, X., Ge, M., Wang, X., Asa-Awuku, A. A., and Tang, M.: Interactions of organosulfates with water vapor under sub- and supersaturated conditions, Atmos. Chem. Phys., 21, 7135–7148, https://doi.org/10.5194/acp-21-7135-2021, 2021.

Pokhrel, R. P., Beamesderfer, E. R., Wagner, N. L., Langridge, J. M., Lack, D. A., Jayarathne, T., Stone, E. A., Stockwell, C. E., Yokelson, R. J., and Murphy, S. M.: Relative importance of black carbon, brown carbon, and absorption enhancement from clear coatings in biomass burning emissions, Atmos. Chem. Phys., 17, 5063–5078, https://doi.org/10.5194/acp-17-5063-2017, 2017.

Saleh, R.: From Measurements to Models: Toward Accurate Representation of Brown Carbon in Climate Calculations, Curr Pollution Rep, 6, 90–104, https://doi.org/10.1007/s40726-020-00139-3, 2020.

Saleh, R., Cheng, Z., and Atwi, K.: The Brown–Black Continuum of Light-Absorbing Combustion Aerosols, Environ. Sci. Technol. Lett., 5, 508–513, https://doi.org/10.1021/acs.estlett.8b00305, 2018.

Saleh, R., Robinson, E. S., Tkacik, D. S., Ahern, A. T., Liu, S., Aiken, A. C., Sullivan, R. C., Presto, A. A., Dubey, M. K., Yokelson, R. J., Donahue, N. M., and Robinson, A. L.: Brownness of organics in aerosols from biomass burning linked to their black carbon content, Nature Geosci, 7, 647–650, https://doi.org/10.1038/ngeo2220, 2014.

Shapiro, E. L., Szprengiel, J., Sareen, N., Jen, C. N., Giordano, M. R., and McNeill, V. F.: Light-absorbing

secondary organic material formed by glyoxal in aqueous aerosol mimics, Atmos. Chem. Phys., 9, 2289–2300, https://doi.org/10.5194/acp-9-2289-2009, 2009.

Song, S., Wang, Y., Wang, Y., Wang, T., and Tan, H.: The characteristics of particulate matter and optical properties of Brown carbon in air lean condition related to residential coal combustion, Powder Technology, 379, 505–514, https://doi.org/10.1016/j.powtec.2020.10.082, 2021.

Stokes, R. H. and Robinson, R. A.: Interactions in Aqueous Nonelectrolyte Solutions. I. Solute-Solvent Equilibria, J. Phys. Chem., 70, 2126–2131, https://doi.org/10.1021/j100879a010, 1966.

Sun, J., Zhang, Y., Zhi, G., Hitzenberger, R., Jin, W., Chen, Y., Wang, L., Tian, C., Li, Z., Chen, R., Xiao, W., Cheng, Y., Yang, W., Yao, L., Cao, Y., Huang, D., Qiu, Y., Xu, J., Xia, X., Yang, X., Zhang, X., Zong, Z., Song, Y., and Wu, C.: Brown carbon's emission factors and optical characteristics in household biomass burning: Developing a novel algorithm for estimating the contribution of brown carbon, Atmos. Chem. Phys., 21, 2329–2341, https://doi.org/10.5194/acp-21-2329-2021, 2021.

Sun, J., Zhi, G., Hitzenberger, R., Chen, Y., Tian, C., Zhang, Y., Feng, Y., Cheng, M., Zhang, Y., Cai, J., Chen, F., Qiu, Y., Jiang, Z., Li, J., Zhang, G., and Mo, Y.: Emission factors and light absorption properties of brown carbon from household coal combustion in China, Atmos. Chem. Phys., 17, 4769–4780, https://doi.org/10.5194/acp-17-4769-2017, 2017.

Tang, J., Li, J., Su, T., Han, Y., Mo, Y., Jiang, H., Cui, M., Jiang, B., Chen, Y., Tang, J., Song, J., Peng, P.'a., and Zhang, G.: Molecular compositions and optical properties of dissolved brown carbon in biomass burning, coal combustion, and vehicle emission aerosols illuminated by excitation–emission matrix spectroscopy and Fourier transform ion cyclotron resonance mass spectrometry analysis, Atmos. Chem. Phys., 20, 2513–2532, https://doi.org/10.5194/acp-20-2513-2020, 2020.

Tian, J., Wang, Q., Ni, H., Wang, M., Zhou, Y., Han, Y., Shen, Z., Pongpiachan, S., Zhang, N., Zhao, Z., Zhang, Q., Zhang, Y., Long, X., and Cao, J.: Emission Characteristics of Primary Brown Carbon Absorption From Biomass and Coal Burning: Development of an Optical Emission Inventory for China, J. Geophys. Res. Atmos., 15, 27,805, https://doi.org/10.1029/2018JD029352, 2019.

Tsigaridis, K. and Kanakidou, M.: The Present and Future of Secondary Organic Aerosol Direct Forcing on Climate, Curr Clim Change Rep, 4, 84–98, https://doi.org/10.1007/s40641-018-0092-3, 2018.

Tuccella, P., Curci, G., Pitari, G., Lee, S., and Jo, D. S.: Direct Radiative Effect of Absorbing Aerosols: Sensitivity to Mixing State, Brown Carbon, and Soil Dust Refractive Index and Shape, J. Geophys. Res. Atmos., 125, 317,

681 https://doi.org/10.1029/2019JD030967, 2020.

682 Turpin, B. J. and Lim, H.-J.: Species Contributions to PM2.5 Mass Concentrations: Revisiting Common

683 Assumptions for Estimating Organic Mass, Aerosol Science and Technology, 35, 602–610,

684 https://doi.org/10.1080/02786820152051454, 2001.

685 Wang, J., Ye, J., Zhang, Q., Zhao, J., Wu, Y., Li, J., Liu, D., Li, W., Zhang, Y., Wu, C., Xie, C., Qin, Y., Lei, Y.,

686 Huang, X., Guo, J., Liu, P., Fu, P., Li, Y., Lee, H. C., Choi, H., Zhang, J., Liao, H., Chen, M., Sun, Y., Ge, X.,

687 Martin, S. T., and Jacob, D. J.: Aqueous production of secondary organic aerosol from fossil-fuel emissions in

688 winter Beijing haze, Proceedings of the National Academy of Sciences of the United States of America, 118,

689 https://doi.org/10.1073/pnas.2022179118, 2021.

690 Wang, Q., Zhou, Y., Ma, N., Zhu, Y., Zhao, X., Zhu, S., Tao, J., Hong, J., Wu, W., Cheng, Y., and Su, H.: Review

691 of Brown Carbon Aerosols in China: Pollution Level, Optical Properties, and Emissions, J. Geophys. Res., 127,

692 455, 2022a.

693 Wang, Q., Wang, L., Gong, C., Li, M., Xin, J., Tang, G., Sun, Y., Gao, J., Wang, Y., Wu, S., Kang, Y., Yang, Y., Li,

694 T., Liu, J., and Wang, Y.: Vertical evolution of black and brown carbon during pollution events over North China

695 Plain, The Science of the total environment, 806, 150950, https://doi.org/10.1016/j.scitotenv.2021.150950, 2022b.

696 Wang, X., Heald, C. L., Ridley, D. A., Schwarz, J. P., Spackman, J. R., Perring, A. E., Coe, H., Liu, D., and Clarke,

697 A. D.: Exploiting simultaneous observational constraints on mass and absorption to estimate the global direct

698 radiative forcing of black carbon and brown carbon, Atmos. Chem. Phys., 14, 10989–11010,

699 https://doi.org/10.5194/acp-14-10989-2014, 2014.

700 Wang, X., Heald, C. L., Liu, J., Weber, R. J., Campuzano-Jost, P., Jimenez, J. L., Schwarz, J. P., and Perring, A.

701 E.: Exploring the observational constraints on the simulation of brown carbon, Atmos. Chem. Phys., 18, 635–653,

702 https://doi.org/10.5194/acp-18-635-2018, 2018.

703 Wang, Y., Wang, Y., Song, S., Wang, T., Li, D., and Tan, H.: Effects of coal types and combustion conditions on

704 carbonaceous aerosols in flue gas and their light absorption properties, Fuel, 277, 118148,

705 https://doi.org/10.1016/j.fuel.2020.118148, 2020.

706 Washenfelder, R. A., Attwood, A. R., Brock, C. A., Guo, H., Xu, L., Weber, R. J., Ng, N. L., Allen, H. M., Ayres,

707 B. R., Baumann, K., Cohen, R. C., Draper, D. C., Duffey, K. C., Edgerton, E., Fry, J. L., Hu, W. W., Jimenez, J.

708 L., Palm, B. B., Romer, P., Stone, E. A., Wooldridge, P. J., and Brown, S. S.: Biomass burning dominates brown

709 carbon absorption in the rural southeastern United States, Geophys. Res. Lett., 42, 653–664,

710 https://doi.org/10.1002/2014GL062444, 2015.

711 Wong, J. P. S., Tsagkaraki, M., Tsiodra, I., Mihalopoulos, N., Violaki, K., Kanakidou, M., Sciare, J., Nenes, A.,

712 and Weber, R. J.: Atmospheric evolution of molecular-weight-separated brown carbon from biomass burning,

713 Atmos. Chem. Phys., 19, 7319–7334, https://doi.org/10.5194/acp-19-7319-2019, 2019.

714 Wu, J., Bei, N., Hu, B., Liu, S., Wang, Y., Shen, Z., Li, X., Liu, L., Wang, R., Liu, Z., Cao, J., Tie, X., Molina, L.

715 T., and Li, G.: Aerosol-photolysis interaction reduces particulate matter during wintertime haze events,

716 Proceedings of the National Academy of Sciences of the United States of America, 117, 9755–9761,

717 https://doi.org/10.1073/pnas.1916775117, 2020.

718 Xie, C., Xu, W., Wang, J., Wang, Q., Liu, D., Tang, G., Chen, P., Du, W., Zhao, J., Zhang, Y., Zhou, W., Han, T.,

719 Bian, Q., Li, J., Fu, P., Wang, Z., Ge, X., Allan, J., Coe, H., and Sun, Y.: Vertical characterization of aerosol optical

720 properties and brown carbon in winter in urban Beijing, China, Atmos. Chem. Phys., 19, 165–179,

721 https://doi.org/10.5194/acp-19-165-2019, 2019.

722 Xie, M., Hays, M. D., and Holder, A. L.: Light-absorbing organic carbon from prescribed and laboratory biomass

723 burning and gasoline vehicle emissions, Scientific reports, 7, 7318, https://doi.org/10.1038/s41598-017-06981-8,

724 2017.

725 Xu, L., Lin, G., Liu, X., Wu, C., Wu, Y., and Lou, S.: Constraining Light Absorption of Brown Carbon in China

726 and Implications for Aerosol Direct Radiative Effect, Geophys. Res. Lett., 51, 455,

727 https://doi.org/10.1029/2024GL109861, 2024.

728 Yan, C., Zheng, M., Bosch, C., Andersson, A., Desyaterik, Y., Sullivan, A. P., Collett, J. L., Zhao, B., Wang, S.,

729 He, K., and Gustafsson, Ö.: Important fossil source contribution to brown carbon in Beijing during winter,

730 Scientific reports, 7, 43182, https://doi.org/10.1038/srep43182, 2017.

731 Yan, J., Wang, X., Gong, P., Wang, C., and Cong, Z.: Review of brown carbon aerosols: Recent progress and

732 perspectives, The Science of the total environment, 634, 1475–1485,

733 https://doi.org/10.1016/j.scitotenv.2018.04.083, 2018.

734 Yang, M., Howell, S. G., Zhuang, J., and Huebert, B. J.: Attribution of aerosol light absorption to black carbon,

735 brown carbon, and dust in China – interpretations of atmospheric measurements during EAST-AIRE, Atmos.

736 Chem. Phys., 9, 2035–2050, https://doi.org/10.5194/acp-9-2035-2009, 2009.

737 Zhang, A., Wang, Y., Zhang, Y., Weber, R. J., Song, Y., Ke, Z., and Zou, Y.: Modeling the global radiative effect

738 of brown carbon: A potentially larger heating source in the tropical free troposphere than black carbon, Atmos.

Chem. Phys., 20, 1901–1920, https://doi.org/10.5194/acp-20-1901-2020, 2020.

Zhang, Q., Streets, D. G., Carmichael, G. R., He, K. B., Huo, H., Kannari, A., Klimont, Z., Park, I. S., Reddy, S., Fu, J. S., Chen, D., Duan, L., Lei, Y., Wang, L. T., and Yao, Z. L.: Asian emissions in 2006 for the NASA INTEX-B mission, Atmos. Chem. Phys., 9, 5131–5153, https://doi.org/10.5194/acp-9-5131-2009, 2009.

Zhang, Q., Li, Z., Shen, Z., Zhang, T., Zhang, Y., Sun, J., Zeng, Y., Xu, H., Wang, Q., Hang Ho, S. S., and Cao, J.: Source profiles of molecular structure and light absorption of PM2.5 brown carbon from residential coal combustion emission in Northwestern China, Environmental pollution (Barking, Essex 1987), 299, 118866, https://doi.org/10.1016/j.envpol.2022.118866, 2022a.

Zhang, W., Wang, W., Li, J., Ma, S., Lian, C., Li, K., Shi, B., Liu, M., Li, Y., Wang, Q., Sun, Y., Tong, S., and Ge, M.: Light absorption properties and potential sources of brown carbon in Fenwei Plain during winter 2018-2019, Journal of environmental sciences (China), 102, 53–63, https://doi.org/10.1016/j.jes.2020.09.007, 2021.

Zhang, Y., Wang, Q., Tian, J., Li, Y., Liu, H., Ran, W., Han, Y., Prévôt, A. S.H., and Cao, J.: Impact of COVID-19 lockdown on the optical properties and radiative effects of urban brown carbon aerosol, Geoscience Frontiers, 13, 101320, https://doi.org/10.1016/j.gsf.2021.101320, 2022b.

Zhao, C., Ruby Leung, L., Easter, R., Hand, J., and Avise, J.: Characterization of speciated aerosol direct radiative forcing over California, J. Geophys. Res., 118, 2372–2388, https://doi.org/10.1029/2012JD018364, 2013.

Zhu, Y., Wang, Q., Yang, X., Yang, N., and Wang, X.: Modeling Investigation of Brown Carbon Aerosol and Its Light Absorption in China, Atmosphere, 12, 892, https://doi.org/10.3390/atmos12070892, 2021.